IEEE Access
Multidisciplinary ⋮ Rapid Review ⋮ Open Access Journal

Received April 28, 2019, accepted May 23, 2019, date of publication June 10, 2019, date of current version June 26, 2019.

Digital Object Identifier 10.1109/ACCESS.2019.2921916

Sensorless Control for Permanent Magnet Synchronous Motor in Rail Transit Application Using Segmented Synchronous Modulation

ZHE CHEN[1], HANG ZHANG[1], WENCONG TU[1], (Student Member, IEEE), GUANGZHAO LUO[1], DARSHAN MANOHARAN[2], AND RALPH KENNEL[2], (Senior Member, IEEE)
[1]School of Automation, Northwestern Polytechnical University, Xi'an 710072, China
[2]Institute for Electrical Drive Systems and Power Electronics, Technische Universitaet Muenchen, 80333 Munich, Germany

Corresponding author: Hang Zhang (wdvvv420@126.com)

This work was supported in part by the National Natural Science Foundation of China under Grant 51707161, in part by the Nature Science Basic Research Plan in Shaanxi Province of China under Grant 2018JQ5187, in part by the Fundamental Research Funds for the Central Universities under Grant 31020170QD029, in part by the Yangtze River Delta Research Institute of NPU, Taicang, in part by the Young Talent Fund of University Association for Science and Technology in Xi'an, and in part by the Shaanxi Key Laboratory of Small and Special Electrical Machine and Drive Technology.

ABSTRACT This paper proposes a position sensorless control technique for permanent magnet synchronous motor (PMSM) used in rail transit application, where a segmented synchronous modulation (SSM) is usually applied. The arbitrary signal injection-based sensorless control is adopted to estimate rotor position. In a switching period, an oversampling technique is used to obtain the average current slope that contains the rotor position information during the active voltage-vector operation. In SSM, the hysteresis zone is set near the carrier ratio (CR) switching critical point to eliminate the influence of the repeated oscillation on the current measurement accuracy. Furthermore, a load disturbance compensation method is designed so that the failure of hysteresis zone is avoided. Through the analysis of power spectral density (PSD) of phase current, the optimization of harmonic energy distribution with hysteresis zone is also verified. The experimental results show that the proposed method can improve the position estimation precision during the fast CR transition, which can be effectively applied in SSM.

INDEX TERMS Permanent magnet synchronous motor (PMSM), segmented synchronous modulation (SSM), arbitrary signal injection, oversampling, sensorless control.

I. INTRODUCTION

High speed railway system employing permanent magnet synchronous machine (PMSM) serves as the electrical traction core in the next generation train. Due to the integration of position sensor and traction motor, the influence brought by the high temperature and mechanical stress causes failure of the mechanical sensors, which leads to traffic safety problems. Therefore, the position sensorless technology is promising and it can solve such problems. In rail transit application, the highest inverter switching frequency is less than 1 kHz because of the limitation caused by switching loss and heat dissipation. Meanwhile, the traction motor has a wide speed range and the maximum fundamental frequency of the motor can reach up to 200 Hz. Therefore, the carrier ratio ($CR = f_c/f_0$) varies greatly throughout the entire speed range. As shown in Figure 1, in order to have better symmetric performance of three-phase currents and make full use of DC bus voltage, a hybrid PWM modulation strategy for traction inverter is widely adopted to meet the low switching-frequency control requirements. It adopts asynchronous space vector modulation (SVM) at low speed, multi-mode synchronous modulation at high speed and square-wave modulation above rated speed [1]–[3].

Generally, the synchronous modulation is subdivided into a regular mode and an optimal PWM mode. So the synchronous modulation is also named as segmented synchronous modulation. As shown in Figure 1, the CR number of the regular mode is odd times of 3, for instance, 21 and 15, then the PWM pulses generated in this way can maintain symmetrical

The associate editor coordinating the review of this manuscript and approving it for publication was Gaolin Wang.

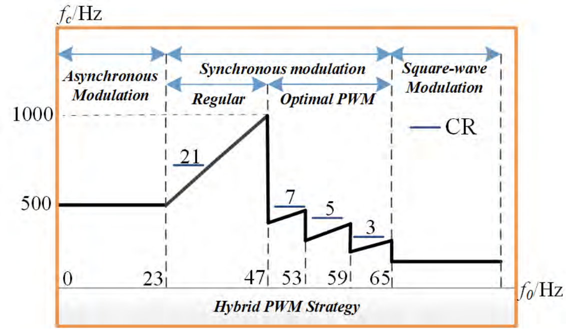

FIGURE 1. Hybrid PWM modulation for high-speed railway traction system.

three-phase output. When CR is less than 10, if the number keeps the same as regular mode, the actual voltage is difficult to reach the command value and the low-order harmonic components increase dramatically due to fewer sampling points. In order to solve this problem under low CR, the optimal PWM is utilized [4], mainly including two methods: current harmonic minimum CHMPWM [5], [6] and selective harmonic elimination SHEPWM [7], [8]. Zhang *et al.* [5] proposes a novel construction of CHMPWM algorithm for the PMSM, which has better harmonic performance at any modulation index and load angle. In [6], a synchronous optimal pulse-width modulation is applied in high-power grinding mills, then a low harmonic current distortion is ensured and the switching losses is also reduced at a very low switching frequency. In [7] and [8], compared with CHMPWM, SHEPWM can eliminate the selective low-order harmonics and its distribution of switching angle in the entire voltage range has good continuity, which is widely used in rail transit traction system and serves as a basic method in this work.

Sensorless control can enhance the reliability and robustness of high-speed rail transit system. Up to now, two categories for implementing sensorless control of PMSM can be found in literature: the fundamental model based method [9], [10] and the saliency tracking based method [3], [11] (In most cases, High Frequency (HF) signal injection is required). The former one is suitable for middle and high speed range and the latter one performs well at standstill and low speed range. As a result, many researchers have proposed a hybrid scheme combining these two methods together and designed a transition region between them [12]. It is a reasonable solution for whole speed range sensorless control, but the stability during the frequent exchange of both methods is still a problem. The arbitrary signal injection method [13], which relies on the measurement of transient current slope during a PWM period, is a new concept for estimating the rotor position and whole speed range applicable. In this work, the arbitrary signal injection method is implemented inside a single FPGA based on current oversampling technique [14].

Remarkably, there are still some difficulties in the application of arbitrary signal injection method in SHEPWM. In general, SHEPWM contains three kinds of frequency division modes, namely, the CR is 7, 5 and 3 respectively. In the sensorless control, the problem of the frequent PWM mode transition exists on account of estimated speed vibrations. It is inevitable that the estimated speed has ripples in steady state, and the fundamental-frequency value is regarded as the transition condition in SHEPWM. In this case, if the transition strategy is not properly designed, this phenomenon leads to frequent transition between different PWM modes, and deteriorates the fitting accuracy of current slope in arbitrary signal injection. Nowadays, many scholars have studied the control performance in SHEPWM [15], [16]. Zhao *et al.* [15] proposes a hybrid SHEPWM scheme for common mode voltage reduction in three-level neutral-point-clamped inverter-based induction motor drives. In [16], a combination of well-known SHE and selective harmonics mitigation (SHM) is designed to shape a spectrum of catenary current harmonics, which can reduce distorting influence of a modern rolling stock supplied by a 3 kV dc catenary on the railway control system. As can be seen, the existing work is mainly about the application of SHEPWM in novel power-circuits or devices, and the optimal synchronous PWM strategies all can greatly improve the current harmonic performance [17]–[19]. However, for the PMSM sensorless control in synchronous modulation region, it is not enough to analyze the control performance of the PWM mode itself. In particular, when the optimal PWM uses SHEPWM, the influence of the different PWM modes transition on the position estimation performance is worth exploring.

TABLE 1. Nomenclature section.

Symbol	Quantity	Unit
θ_e	electrical rotor position	rad
$\boldsymbol{u}_s^s$	stator voltage	V
R_s	stator resistance	Ω
$\boldsymbol{L}_s^s$	stator inductance	H
ψ_{PM}^r	rotor flux linkage	Wb
Y_Σ	position independent part of stator admittance	S
Y_Δ	position dependent part of stator admittance	S
T_s	sampling time	μs
Δi_s^s	current rise in a sampling time	A
$\Delta i_{s,HF}^s$	active voltage vector excited current difference	A
$\Delta i_{s,LF}^s$	zero voltage vector excited current difference	A
$\Delta i_{s,\Sigma}^s$	isotropic current rise in a sampling time	A
ε_s^α, ε_s^β	current difference caused by saliency in $\alpha\beta$-axis	V
u_s^α, u_s^β	stator voltage in $\alpha\beta$-axis	V
$\hat{\theta}_e$	estimated rotor position	rad
ξ_s^α	current slope during zero voltage vector in α-axis	Numerical
$i_{s,0}^\alpha$	current offset obtained by recursive method in α-axis	A
t_{act}	duration time of active voltage vector	μs
t_{zero}	duration time of zero voltage vector	μs
T_{int}	period of interrupt signal	μs

In order to eliminate such influence, this paper proposes a hysteresis zone design in the segmented synchronous region and corresponding SHEPWM pattern implementation is realized as well. Experimental results demonstrated that the position estimation accuracy is improved and the transition between different PWM modes is smoother.

Nomenclature for the sensorlss method is as TABLE1.

II. SALIENCY EFFECT FOR SENSORLESS CONTROL

The machine saliency is parameter independent and thus reliable for position estimation. It is theoretically valid for the whole speed range. The transformation matrix $\boldsymbol{T}$ transfers equations from rotor coordinate to stator coordinate, and its derivative $\frac{\mathrm{d}}{\mathrm{d}t}\boldsymbol{T}$ are given by

$$\boldsymbol{T} = \begin{bmatrix} \cos\theta_e & -\sin\theta_e \\ \sin\theta_e & \cos\theta_e \end{bmatrix}, \tag{1}$$

$$\frac{\mathrm{d}}{\mathrm{d}t}\boldsymbol{T} = \omega_e \begin{bmatrix} -\sin\theta_e & -\cos\theta_e \\ \cos\theta_e & -\sin\theta_e \end{bmatrix} = \omega_e\acute{\boldsymbol{T}}, \tag{2}$$

with θ_e being the electrical rotor position and a derivative with respect to the electrical position $\frac{\mathrm{d}}{\mathrm{d}\theta_e}\boldsymbol{X}$ is denoted by a prime $\acute{\boldsymbol{X}}$. So, $\frac{\mathrm{d}}{\mathrm{d}t}\boldsymbol{T} = \omega_e = \omega_e\acute{\boldsymbol{T}}$

Then stator voltage can be represented by

$$\begin{aligned} \boldsymbol{u}_s^s &= R_s\boldsymbol{i}_s^s + \boldsymbol{L}_s^s\frac{\mathrm{d}}{\mathrm{d}t}\boldsymbol{i}_s^s + \omega_e\acute{\boldsymbol{L}}_s^s\boldsymbol{i}_s^s + \omega_e\acute{\boldsymbol{T}}\boldsymbol{\psi}_{PM}^r, \\ \boldsymbol{L}_s^s &= \begin{bmatrix} L_s^d\cos^2\theta_e + L_s^q\sin^2\theta_e & \left(L_s^d - L_s^q\right)\sin\theta_e\cos\theta_e \\ \left(L_s^d - L_s^q\right)\sin\theta_e\cos\theta_e & L_s^d\sin^2\theta_e + L_s^q\cos^2\theta_e. \end{bmatrix} \end{aligned} \tag{3}$$

and the current derivative can be solved from (3)

$$\frac{\mathrm{d}}{\mathrm{d}t}\boldsymbol{i}_s^s = [Y_\Sigma\boldsymbol{I} + Y_\Delta\boldsymbol{S}(\theta_e)] \cdot \left[\boldsymbol{u}_s^s - R_s\boldsymbol{i}_s^s - \omega_e\left(\acute{\boldsymbol{T}}\boldsymbol{\psi}_{PM}^r + \acute{\boldsymbol{L}}_s^s\boldsymbol{i}_s^s\right)\right], \tag{4}$$

with the rotor position independent part of stator admittance $Y_\Sigma = \frac{1}{2}\left(\frac{1}{L_s^d} + \frac{1}{L_s^q}\right)$, the position dependent part of stator admittance $Y_\Delta = \frac{1}{2}\left(\frac{1}{L_s^d} - \frac{1}{L_s^q}\right)$ and the position dependent transformation matrix $\boldsymbol{S}(\theta_e) = \begin{bmatrix} \cos(2\theta_e) & \sin(2\theta_e) \\ \sin(2\theta_e) & -\cos(2\theta_e) \end{bmatrix}$.

According to (4) the discrete function can be obtained

$$\begin{aligned} \Delta\boldsymbol{i}_s^s[n] = [Y_\Sigma\boldsymbol{I} + Y_\Delta\boldsymbol{S}(\theta_e)] \cdot T_s \cdot \Big[&\boldsymbol{u}_s^s[n_1] - R_s\boldsymbol{i}_s^s[n_1] - \omega_e[n_1] \\ &\times \left(\acute{\boldsymbol{T}}[n_1]\boldsymbol{\psi}_{PM}^r + \acute{\boldsymbol{L}}_s^s[n_1]\boldsymbol{i}_s^s[n_1]\right)\Big], \end{aligned} \tag{5}$$

where $\Delta\boldsymbol{i}_s^s[n] = \boldsymbol{i}_s^s[n] - \boldsymbol{i}_s^s[n_1]$ and $[n_x] = [n - x]$ represents the intervals in the past, T_s is the traditional sampling time of system (once per interrupt period). Furthermore, (5) can be divided into active voltage vector excited current difference $\Delta\boldsymbol{i}_{s,HF}^s[n]$ and zero voltage vector excited current difference $\Delta\boldsymbol{i}_{s,LF}^s[n]$, as follows.

$$\Delta\boldsymbol{i}_{s,HF}^s[n] = [Y_\Sigma\boldsymbol{I} + Y_\Delta\boldsymbol{S}(\theta_e)] \cdot \boldsymbol{u}_s^s[n_1] \cdot T_s, \tag{6}$$

$$\begin{aligned} \Delta\boldsymbol{i}_{s,LF}^s[n] = [Y_\Sigma\boldsymbol{I} + Y_\Delta\boldsymbol{S}(\theta_e)] \cdot T_s \cdot \Big[&R_s\boldsymbol{i}_s^s[n_1] + \omega_e[n_1] \\ &\times \left(\acute{\boldsymbol{T}}[n_1]\boldsymbol{\psi}_{PM}^r + \acute{\boldsymbol{L}}_s^s[n_1]\boldsymbol{i}_s^s[n_1]\right)\Big] \cdot T_s, \end{aligned} \tag{7}$$

Neglecting the position dependent admittance part Y_Δ for the component excited by active voltage vector, the rotor position independent component of stator current rise can be expressed as

$$\Delta\boldsymbol{i}_{s,\Sigma}^s[n] = Y_\Sigma\boldsymbol{u}_s^s[n_1]T_s - \Delta\boldsymbol{i}_{s,LF}^s[n], \tag{8}$$

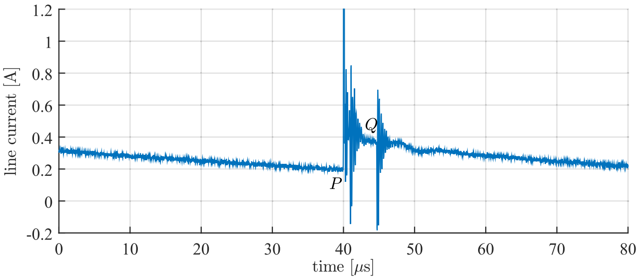

FIGURE 2. Actual α-axis current variation during active voltage vector.

Subtracting the isotropic current rise $\Delta\boldsymbol{i}_{s,\Sigma}^s[n]$ from the total current rise $\Delta\boldsymbol{i}_s^s[n]$, the position dependent current difference can be given as

$$\boldsymbol{\varepsilon}_s^s[n] = \Delta\boldsymbol{i}_s^s[n] - \Delta\boldsymbol{i}_{s,\Sigma}^s[n] = Y_\Delta\boldsymbol{S}(\theta_e)\,\boldsymbol{u}_s^s[n_1]T_s. \tag{9}$$

At last the position dependent admittance Y_Δ and the sampling time T_s are eliminated by division

$$\frac{\varepsilon_s^\alpha}{\varepsilon_s^\beta} = \frac{u_s^\alpha + u_s^\beta\tan(2\theta_e)}{u_s^\alpha\tan(2\theta_e) - u_s^\beta}. \tag{10}$$

And the estimated rotor position can be calculated (please refer [20] for more information)

$$\hat{\theta}_e = \frac{1}{2}\arctan\left(\frac{u_s^\alpha\varepsilon_s^\beta + u_s^\beta\varepsilon_s^\alpha}{u_s^\alpha\varepsilon_s^\alpha - u_s^\beta\varepsilon_s^\beta}\right). \tag{11}$$

As usual for saliency based methods, the modulo of ±90° requires post processing.

III. ARBITRARY SIGNAL INJECTION METHOD

In arbitrary signal injection method, an additional injection signal is not necessary for current excitation. The intrinsic active vector of PWM signal during normal operation caused current difference contains the rotor position information because of the saliency effect. However, the current derivative during active voltage vectors can not be measured directly due to oscillation and limited time instance. Figure 2 shows that both current values, at point P and Q, cannot be measured in noise environment.

An alternative method measuring the current slope during zero voltage vector by means of current oversampling is introduced in [20]. Firstly, current values during zero voltage vector are oversampled, then the current slope $\xi_s^\alpha[n]$, $\xi_s^\alpha[n_1]$ and the current offset $i_{s,0}^\alpha[n]$, $i_{s,0}^\alpha[n_1]$ are obtained through recursive calculation. $t_{act}[n]$ is the duration of active voltage vector. The visual explanation of these quantities is demonstrated in Figure 3.

The value of zero voltage vector duration is given

$$t_{zero}[n] = T_{int} - t_{act}[n], \tag{12}$$

where T_{int} is the period of interrupt signal. Therefore, the active vector of PWM signal caused current difference

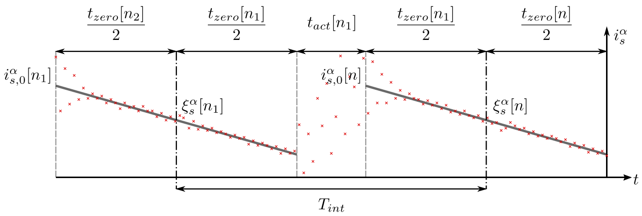

FIGURE 3. Information in the zero voltage vector straights.

can be calculated

$$\Delta \boldsymbol{i}_s^{s\prime}[n]=\boldsymbol{i}_{s,0}^{s}[n]-\left(\boldsymbol{i}_{s,0}^{s}[n_1]+\boldsymbol{\xi}_s^s[n_1]\frac{1}{2}(t_{zero}[n_2]+t_{zero}[n_1])\right), \tag{13}$$

Note that $\Delta \boldsymbol{i}_s^{s\prime}$ is the active voltage caused current difference during active vector, it doesn't equal the current difference caused by average supplied voltage during the whole PWM cycle $\Delta \boldsymbol{i}_s^s$. Actually, $\Delta \boldsymbol{i}_s^{s\prime}$ has a phase lead for $\frac{\pi}{2}$ compared with $\Delta \boldsymbol{i}_s^s$.

The current slope during zero voltage vector $\boldsymbol{\xi}_s^s$ theoretically equals the negative value of zero voltage excited component $\Delta \boldsymbol{i}_{s,LF}^s$. In particular it is assumed that between point P and Q, $\Delta \boldsymbol{i}_{s,LF}^s$ can be transformed as

$$\Delta \boldsymbol{i}_{s,LF}^{s}{}'[n] = -\frac{1}{2}(\boldsymbol{\xi}_s^s[n_1] + \boldsymbol{\xi}_s^s[n])t_{act}[n_1]. \tag{14}$$

Then according to (8) and (9) the saliency cause current difference is

$$\boldsymbol{\varepsilon}_s^{s\prime}[n_1] = \Delta \boldsymbol{i}_s^{s\prime}[n] - Y_\Sigma \boldsymbol{u}_s^{s\prime}[n_1]t_{act}[n_1] + \Delta \boldsymbol{i}_{s,LF}^{s}{}'[n]. \tag{15}$$

which requires only one motor parameter, the rotor position independent component of stator admittance Y_Σ. Here must note that $\boldsymbol{u}_s^{s\prime}$ is the average stator voltage during active vector, not the PWM represented stator voltage $\boldsymbol{u}_s^s$, which is the average voltage during whole PWM cycle. Equation (16) gives the relationship between those voltages

$$\boldsymbol{u}_s^{s\prime} t_{act} = \boldsymbol{u}_s^s T_{int}. \tag{16}$$

At last the rotor position $\hat{\theta}_e'$ is estimated by arctan function. $\hat{\theta}_e' = \frac{1}{2}\arctan\left(\frac{u_s^\alpha \varepsilon_s^\beta + u_s^\beta \varepsilon_s^\alpha}{u_s^\alpha \varepsilon_s^\alpha - u_s^\beta \varepsilon_s^\beta}\right)$ Because of the phase difference between $\Delta \boldsymbol{i}_s^{s\prime}$ and $\Delta \boldsymbol{i}_s^s$, the relationship between $\hat{\theta}_e'$ and rotor position $\hat{\theta}_e$ is given

$$\theta_e = \hat{\theta}_e' + \frac{\pi}{2}. \tag{17}$$

Note that now $\theta_e \in [0, \pi]$ requires post processing.

Since the arbitrary injection method estimate rotor position based on current difference which is caused by active vector of PWM signal, at low speed range without load and at standstill the active voltage is so small that a valid current rise cannot be measured. Therefore, the performance of arbitrary injection method deteriorate at low speed range without load and invalid at standstill.

IV. SENSORLESS CONTROL IN SEGMENTED SYNCHRONOUS MODULATION

A. REGULAR MODE

For the synchronous modulation, the position of command voltage vector is fixed and distributed evenly, in other words, the composite vector rotates at equal angular intervals. When the fundamental frequency is high, this modulation mode ensures three-phase symmetry of the output-voltage and eliminates parasitic harmonics. In general, the number of voltage vectors in each fundamental period is the CR number. In this paper, CR of the regular mode is 21, and the command voltage in each sector is synthesized by two basic vectors and zero vectors. Here, the angular interval $\Delta\theta$ is 17°, as shown in Figure 4, and the fitting position of the vector can be obtained by accumulating $\Delta\theta$ in sequence. When the total accumulated angle θ_{sum} exceeds 60°, one is added to the sector value and θ_{sum} subtracts 60°. Then, a new sector angle calculation process is started. Because the angle and sector are calculated separately, the calculation-way of voltage vector operational-time in regular synchronous mode is the same as asynchronous modulation.

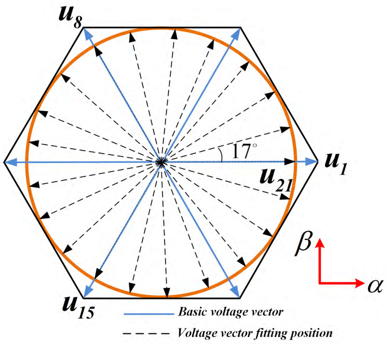

FIGURE 4. Command voltage vector distribution when using 21-pulse synchronous modulation.

B. SHEPWM

When the CR is less than 10, the SHEPWM is used to eliminate the undesired low-order harmonics in the output voltage so that reference voltage can be tracked well. Because the 3th harmonics cancele each other in the line-voltage, SHE aims to eliminate the odd-order harmonics that are not integer multiple of 3 in the phase-voltage. Remarkably, the calculation of switching angle and the generation of three-phase pulses are the design difficulties in the SHEPWM. Figure 5 shows the output voltage of this modulation method, where T_f is fundamental-period, the pulse number and CR are both $2N+1$.

The Fourier Series expansion equation of the A-phase voltage can be expressed as

$$u_{AO} = \sum_{k=1}^{\infty}(a_k \cos k\omega t + b_k \sin k\omega t) \tag{18}$$

Because the phase voltage is even symmetric in the 1/4 period, the actual voltage contains only sin-item and

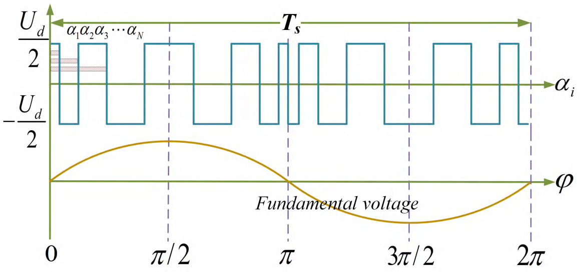

FIGURE 5. Output A-phase voltage when using SHEPWM.

odd-order harmonics. Then, in equation (18), $a_k = 0$ and the following expression can be obtained

$$b_k = -\frac{2u_{dc}}{k\pi}\left[1 + 2\sum_{i=1}^{N}(-1)^i \cos k\alpha_i\right] \tag{19}$$

where k is odd, N is the number of switch angles in 1/4 fundamental period and satisfies $\alpha_1 < \alpha_2 < \alpha_3 \cdots < \alpha_N$. Under this constraint, the output voltage pulse can be obtained by solving the value from α_1 to α_N, which effectively controls the amplitude of the fundamental voltage and eliminates $N-1$ selective harmonics.

The 7-pulse SHE is used to eliminate the 5^{th} and 7^{th} harmonics that are relatively rich in the low-order components. According to equation (19), under this PWM mode, the switching angle equation can be expressed as

$$\begin{cases} -1 + 2\cos\alpha_1 - 2\cos\alpha_2 + 2\cos\alpha_3 = M \\ -1 + 2\cos 5\alpha_1 - 2\cos 5\alpha_2 + 2\cos 5\alpha_3 = 0 \\ -1 + 2\cos 7\alpha_1 - 2\cos 7\alpha_2 + 2\cos 7\alpha_3 = 0 \end{cases} \tag{20}$$

where M is modulation depth, and its resolution is 0.01.

For the 5- and 3-pulse SHE modes, there are respectively two and one switching angles in the 1/4 fundamental period. Unlike the initial negative step of the 7- and 3-pulse modes, the 5-pulse SHE has an initial forward step, therefore, the corresponding negative sign on the right side of equation (20) should be removed. The 3-pulse SHE directly controls the amplitude of the fundamental wave and can achieve a smooth transition to the square-wave modulation. The switching angle equations of 5- and 3-pulse mode can be written as

$$\begin{cases} 1 - 2\cos\alpha_1 + 2\cos\alpha_2 = M \\ 1 - 2\cos 5\alpha_1 + 2\cos 5\alpha_2 = 0 \end{cases} \tag{21}$$

$$-1 + 2\cos\alpha_1 = M \tag{22}$$

In the above three kinds of SHE modes, the switching angles are calculated offline through the Fsolve function in MATLAB. In order to obtain the optimal solution, the initial switching angle can be selected as

$$\underbrace{\begin{cases} \alpha_i = 60^\circ \cdot i/N (i = 2, 4, 6\cdots, i \le N) \\ \alpha_i = 60^\circ \cdot (i-1)/N (i = 1, 3, 5\cdots, i \le N) \end{cases}}_{N\ is\ even} \tag{23}$$

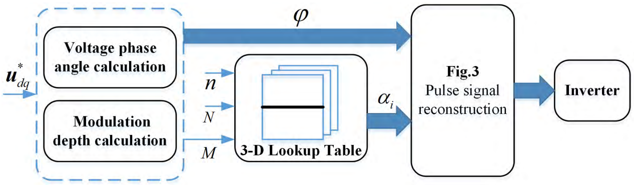

FIGURE 6. Digital implementation process of SHEPWM.

$$\underbrace{\begin{cases} \alpha_i = \alpha_{i+1} = 60^\circ \cdot (i+1)/(N+1) \\ \alpha_N = 60^\circ \end{cases}}_{N\ is\ odd} \tag{24}$$

Figure 6 shows the implementation process of SHEPWM, where $M = \pi\sqrt{u_d^2 + u_q^2}\Big/2U_{dc}$, φ is fundamental voltage phase angle. Here, all switching angles with different M value are divided into multiple arrays and stored in the look-up table module, and n represents the number of the arrays.

C. ARBITRARY SIGNAL INJECTION WITH HYSTERESIS FREQUENCY REGION

The premise of arbitrary signal injection method implement is that the fundamental current can be oversampled in one switching period. So, the frequent PWM modes transition caused by the small change of the estimated speed affects the accurate control of the output voltage-phase and reduce the oversampling accuracy, resulting in a position estimation error.

Taking the transition between SHE7 and SHE5 as an example demonstrated in Figure 7, due to small vibration in the estimated speed whose frequency is selected as the transition condition, the frequent transition occurs between SH7 and SHE5, which affects the output voltage stability. The effectiveness of arbitrary signal injection method depends on the sampled current signal. Thus, when the PWM mode changes frequently, the current signal also fluctuates similarly.

In order to eliminate the oversampling error of current signal, Figure 8 shows the design principle of the proposed hysteresis zone in the sensorless method. Obviously, when the hysteresis zone is not used, the current slope accuracy is distorted, which affects the position estimation accuracy.

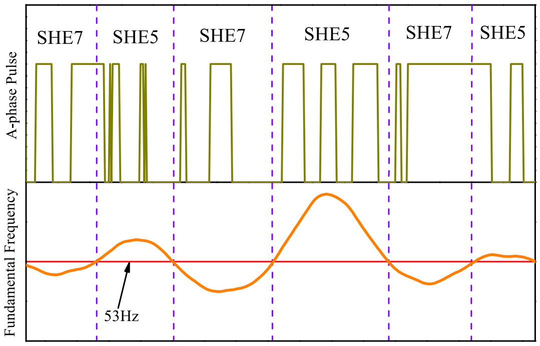

FIGURE 7. Modulation mode change caused by small fluctuations in estimated speed.

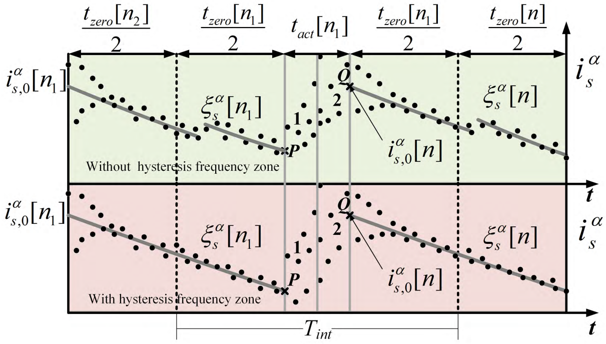

FIGURE 8. Influence of hysteresis frequency setting on arbitrary signal injection method.

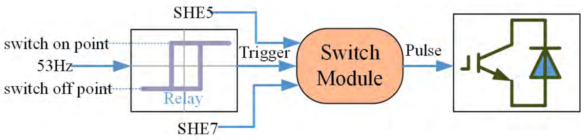

FIGURE 9. Implementation of frequency hysteresis zone.

After using the hysteresis zone, the original judgment frequency line is transformed to a frequency band. From SHE7 to SHE5, the PWM mode is set as SHE7 in hysteresis zone so that it can achieve the ideal transition condition. Therefore, the accuracy of the current slope is significantly improved.

Figure 9 reveals the implementation of frequency hysteresis zone in the digital system. The ideal frequency line is 53Hz. Through a relay module, the actual transition frequency from SHE7 to SHE5 is 54.5Hz, conversely, the frequency is 51.5Hz. In actual operation, the range of estimated speed fluctuation between different PWM modes is not fixed due to the difference of harmonic components. In order to complete the transition faster, the hysteresis frequency is also different. The transition frequency band is shown in TABLE 2.

TABLE 2. Selected hysteresis frequency.

Transition State	Frequency band width
21-pulse SVM to SHE7	2Hz
SHE7 to SHE5	3Hz
SHE5 to SHE3	3.5Hz

D. DESIGN OF A LOAD DISTURBANCE COMPENSATION

In the SHEPWM-based sensorless control, as shown in Fig.1, the transition fundamental frequency of SHE7, SHE5 and SHE3 is 47Hz, 53Hz and 59Hz respectively. Taking the transition between SHE7 and SHE5 as an example, when the inverter operates in steady state with SHE5 mode, the load sudden increase causes the estimated speed fluctuation to exceed the range of the hysteresis frequency region, then the inverter enters the SHE7 mode, as shown in Figure10. In this case, the hysteresis effect is invalidated, and the position estimation accuracy is affected as well.

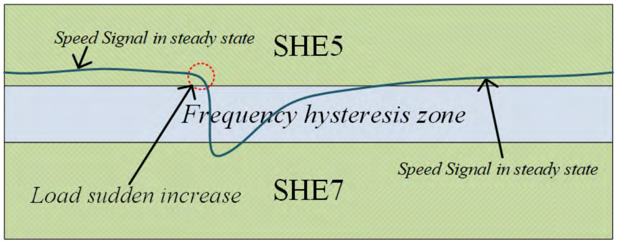

FIGURE 10. Influence of load-disturbance on hysteresis frequency zone.

In order to eliminate the influence of load disturbance on the stability of the PWM mode, the load torque feed-forward compensation is proposed so that the hysteresis can be maintained at all times. Here, a load torque sliding mode observer is designed. In the process, $i_d^* = 0$, the following state equation can be obtained

$$\begin{cases}\dot{\omega}_e = \dfrac{1.5P_p^2\psi_f}{J} i_q - \dfrac{P_p}{J}T_{Load}\\ \dot{T}_{Load} = 0\end{cases} \tag{25}$$

where ω_e is electrical angular speed, ψ_f is flux linkage, P_p is pole pairs, i_q is actual q-axis current, J is inertia and T_{Load} represents the load torque.

In a control period, the load torque can be regarded as a constant. Then, the load-disturbance SMO can be constructed as

$$\begin{cases}\dot{\hat{\omega}}_e = \dfrac{1.5P_p^2\psi_f}{J} i_q - \dfrac{P_p}{J}\hat{T}_{Load} + V\\ \dot{\hat{T}}_{Load} = \eta V\end{cases} \tag{26}$$

where $V = k * sigmoid\left(\hat{\omega}_e - \omega_{actual}\right)$, k is the sliding mode gain, η is feedback gain, $\hat{\omega}_e$ and $\hat{T}_{Load}$ are estimated electrical angular speed and load torque that calculated by (26). In order to suppress the chattering, the conventional sign function is replaced by sigmoid function so that the width of the boundary layer becomes wider. Fig.11 shows the load torque estimation process. By combining the arbitrary signal injection with load estimation, the proposed sensorless control strategy based on SHEPWM is presented in Fig.12, where β is voltage phase angle in dq-axis and φ is pulse generation angle in ABC-axis, $i_{q\_com} = k_L\hat{T}_{Load}$, k_L is compensation gain.

In Fig.11, the sliding mode surface can be selected as $s = E_1 = \hat{\omega}_e - \omega_{actual}$, and $E_2 = \hat{T}_{Load} - T_{Load}$. Combined with(26), the following error equation can be

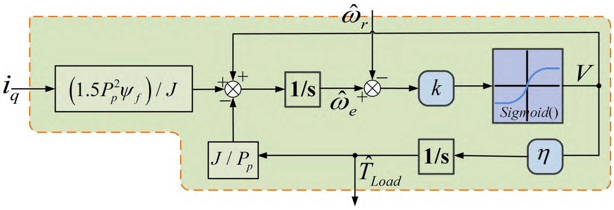

FIGURE 11. Load torque estimation process based on SMO.

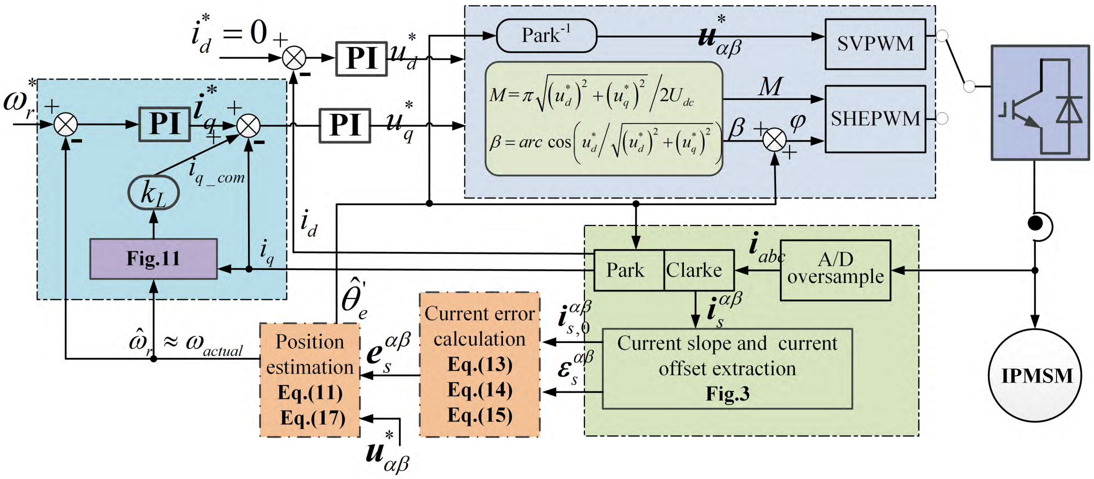

FIGURE 12. Proposed sensorless control strategy based on SHEPWM.

TABLE 3. Parameters of the SPMSM.

Parameter	Value
DC link voltage	582 V
Rated power	2.2 kW
Stator resistance	2.05 Ω
Stator inductance	14.4 mH
Pole pairs	3
Rated speed	3000.0 r/min
Rated torque	7.1 Nm
Total moment of inertia	0.009 Kg.m^2

obtained

$$\begin{cases}\dot{E}_1 = -\dfrac{P_p}{J}E_2 + V\\ \dot{E}_2 = \eta V\end{cases} \tag{27}$$

According to the stability conditions of the sliding mode, the following in-equation can be given

$$s\dot{s} = E_1\dot{E}_1 = E_1\left[k*sigmoid\left(E_1\right) - \left(P_p/J\right)E_2\right] \le 0 \tag{28}$$

where $k = -L\left|\left(P_p/J\right)E_2\right|$, $L \ge 1$. When the SMO arrives the sliding mode surface, $s = \dot{s} = 0$, then the following load error equation can be obtained from equation(27).

$$\dot{E}_2 - \left(\eta P_p/J\right)E_2 = 0 \tag{29}$$

Furthermore, (29) can be transformed as

$$E_2 = \mu\exp\left(\frac{\eta P_p}{J}t\right) \tag{30}$$

where $\eta < 0$, μ is constant. The load observed error E_2 changes exponentially to zero with t, and the approach speed is determined by the feedback gain η. Therefore, according to the selection range of k and η, the SMO can be kept stable and the load torque can be accurately observed.

E. THE EFFECT OF HYSTERESIS FREQUENCY ZONE ON HARMONIC ENERGY DISTRIBUTION

When the motor operates at transition fundamental frequency, without hysteresis frequency zone, frequent PWM modes transition causes instability of harmonic energy distribution. In order to analysis the effect of hysteresis frequency zone on the energy distribution, the power spectral density (PSD) of the phase current is selected as a comparison indicator. When the fundamental frequency is fixed, PSD of phase-current can be expressed as

$$S(f) = \begin{cases}\dfrac{1}{T^2}\left|I_T(F)\right|^2 & F = \dfrac{N}{T}\\ 0 & others\end{cases} \tag{31}$$

where $N = 0, 1, 2, 3\cdots$, T and F are fundamental current period and frequency respectively, $I_T(F)$ is the Fourier transform of current signal in one period. Obviously, the PSD only contains discrete components, here, the $I_T(F)$ can be transformed as

$$\begin{aligned} I_T(NF) &= \frac{2 - 2\cos(T\pi NF) - T\pi F\sin(T\pi NF)}{T\pi^2(NF)^2}e^{-j\pi TNF}\\ &= \begin{cases}-\dfrac{4}{N^2\pi^2F} & when\,N\ is\ odd\\ 0 & when\,N\ is\,even\end{cases} \end{aligned} \tag{32}$$

In SHEPWM-based sensorless control, PSD is mainly concentrated on the fundamental frequency and its odd-order harmonics. Fig.13 shows the comparison of PSD before and after using hysteresis frequency zone. As can be seen, when the motor operates at 53Hz, after hysteresis frequency zone setting, the PSD amplitude of 7th harmonics drops by 11dB. It means that when the motor speeds up to 1060r/min, the harmonic components do not change repeatedly due to the existence of the hysteresis zone, and the PSD distribution conforms to the harmonic characteristics of the 7-pulse SHE. Similarly, when the motor operates at 59Hz, PSD amplitude of 5th,7th and 11th harmonics all are reduced after using hysteresis zone. So, the frequent harmonics energy changes can be avoided.

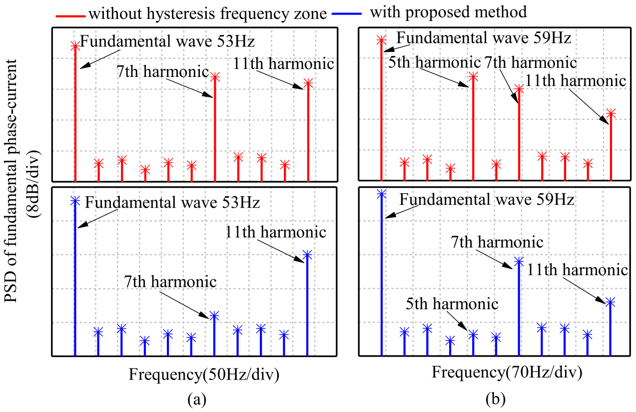

FIGURE 13. PSD comparision between the two case that without- and with hysteresis frequency zone in sensorless control. (a) Operating at 1060r/min. (b) Operating at 1180r/min.

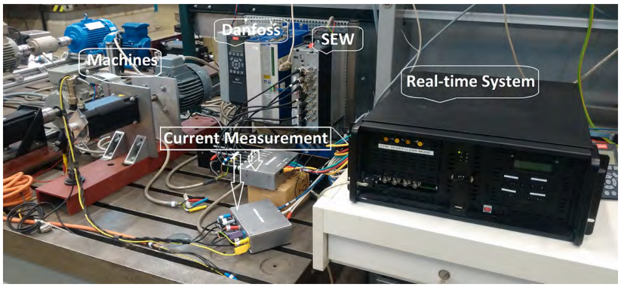

FIGURE 14. The used testbench.

V. EXPERIMENTAL RESULTS

The used test bench composes of a real-time computer system involving an FPGA as core controller, two machines with coupled rotor shafts, two two-level inverters and measurement devices, which are shown in Figure 14. The control-side 5kW inverter is manufactured and modified by the company SEW® and it provides full control of the upper side 3 IGBT gates and the other 3 PWM signals for the lower side 3 IGBTs are generated by the SEW® inverter itself. The dead-time is 0.8 μs. Consequently, only 3 channel PWM signals produced by the real time system are fed to the control-side SEW® inverter to implement any control algorithm. The load-side 5kW inverter is made by the company Danfoss® and it is equipped with a micro-controller and can be configured manually through a front-panel and an LCD display. It drives a load-side induction machine.

The FPGA has its fast oversampling ability and parallel calculation advantage. Field oriented control (FOC) and arbitrary signal injection method are implemented all in VHDL code. FOC runs in 2MHz and current oversampling runs in 20MHz to guarantee enough effective data. Detailed FPGA implementation can be found in [14].

A. STEADY STATE PERFORMANCE

Fig.15 shows the steady state performance of sensorless control when fundamental frequency is 53Hz. As can be seen, without hysteresis frequency zone, the induced fundamental current continuously switches between the SHE7 and SHE5. The actual speed and estimated position both fluctuate during the process, and the maximum position estimation error arrives 0.3rad. After using hysteresis frequency zone, since the upper limit of the hysteresis frequency range has not been reached, the phase current can be stably maintained in SHE7 mode, and the position estimation accuracy is also improved. In the PSD performance comparison, with hysteresis frequency zone, the harmonics energy amplitude is significantly reduced, which means that the repeated changes in harmonic components are eliminated.

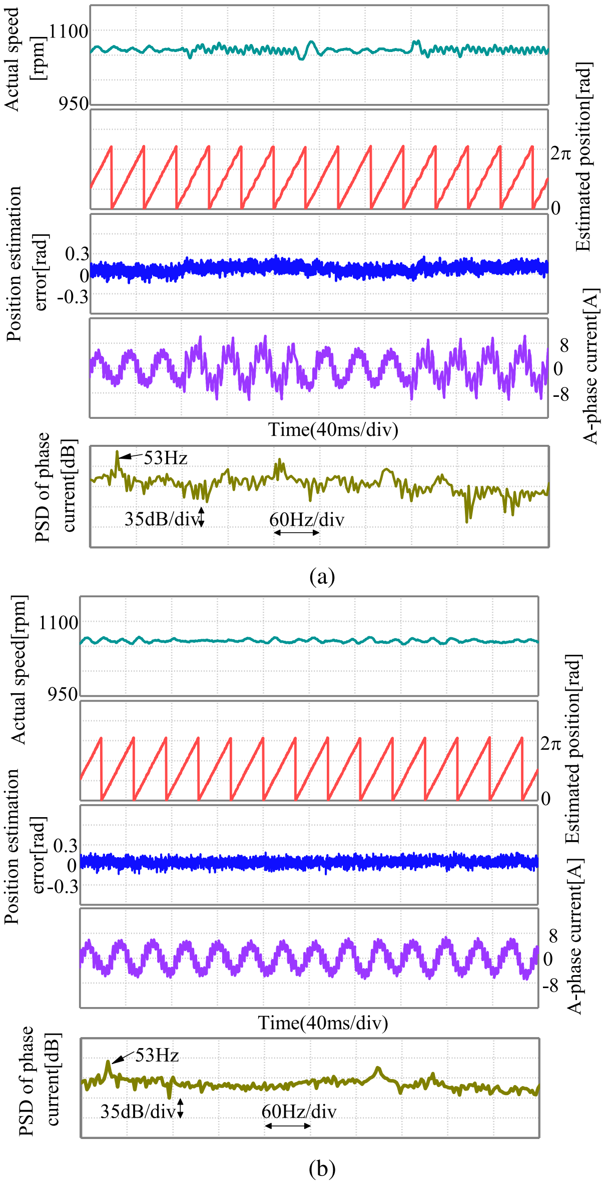

FIGURE 15. Sensorless operation at 1060 r/min with rated load. (a) Without hysteresis frequency zone. (b) With hysteresis frequency range = 3Hz.

The sensorless performance comparison at 1180r/min is given in Fig.16. After using hysteresis frequency zone, the speed and position estimation performance both are

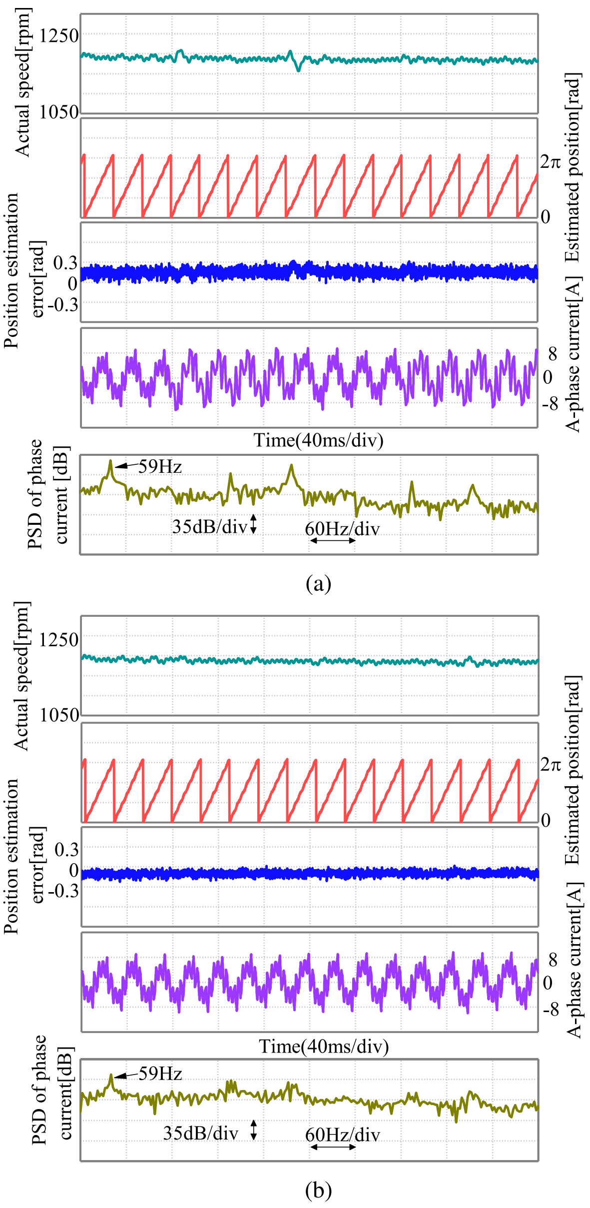

FIGURE 16. **Sensorless operation at 1180 r/min with rated load. (a) Without hysteresis frequency zone (b) With hysteresis frequency range = 3.5Hz.**

improved, and the position estimation error can be always controlled within 0.15rad. For the PSD amplitude, the 5th harmonic is reduced obviously, which is consistent with Fig.13(b).

B. DYNAMIC STATE PERFORMANCE

With hysteresis frequency zone, as TABLE 2, Fig.17 shows the speed response of sensorless control with rated load. The tested IPMSM operates from 500 to 1200r/min, which covers the speed range in SHEPWM mode. It can be seen that position estimation error is within 0.15rad during the speed changing. The A-phase current also maintains good stability throughout the process.

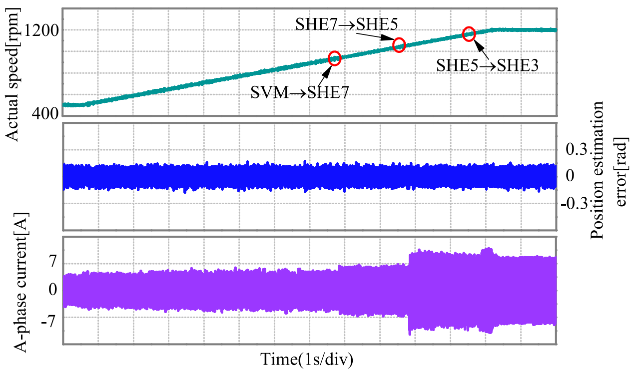

FIGURE 17. **Hysteresis-based sensorless operation with rated load when the speed response changes from 500r/min to 1200r/min.**

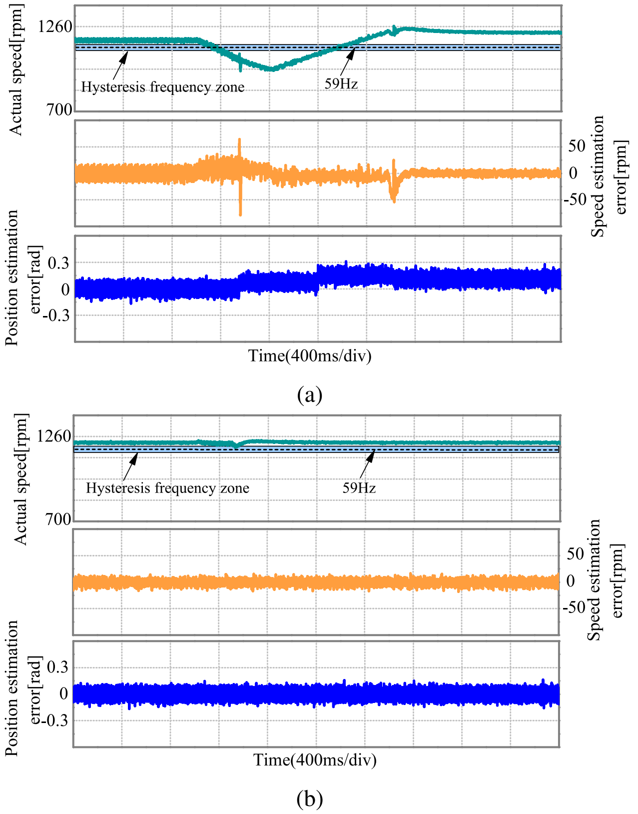

FIGURE 18. **Sensorless operation at 1180 r/min with rated load. (a) Without hysteresis frequency zone. (b) With hysteresis frequency range = 3.5Hz.**

When IPMSM operates at a constant speed with sudden load increase, the hysteresis frequency region is disabled and causes a change in the modulation mode, as shown in Fig.10, which makes the sensorless control performance unstable. Fig.18 shows the load-disturbance compensation results, and load changes from empty to rated value. Obviously, after compensation, the speed fluctuation dose not exceeds the hysteresis frequency region between SHE5 and SHE3, speed- and position-estimation errors both are reduced, which can be controlled in 20r/min and 0.15rad respectively in all dynamic process.

VI. CONCLUSION

Based on arbitrary signal injection method, this paper proposes a sensorless control strategy that is suitable for segmented synchronous modulation. The current oversampling technique is used to detect the current change rate excited by the fundamental modulation voltage during one PWM operation period, and then the difference between the current and the ideal non-salient model is used to obtain the salient signal, which can be reflected by current change rate. Considering the frequent transition of PWM modes in the segmented synchronous modulation, a hysteresis zone is set near the transition point to make the current smoother and improve the position estimation accuracy. Furthermore, a load-disturbance compensation method is designed to avoid the failure of hysteresis zone, and the influence of hysteresis zone on PSD of phase-current is also analyzed. Experiments proved the effectiveness of the proposed method.

REFERENCES

[1] H. Yang, Y. Zhang, G. Yuan, P. D. Walker, and N. Zhang, "Hybrid synchronized PWM schemes for closed-loop current control of high-power motor drives," *IEEE Trans. Ind. Electron.*, vol. 64, no. 9, pp. 6920–6929, Sep. 2017.

[2] C. Wang, K. Wang, and X. You, "Research on synchronized SVPWM strategies under low switching frequency for six-phase VSI-fed asymmetrical dual stator induction machine," *IEEE Trans. Ind. Electron.*, vol. 63, no. 11, pp. 6767–6776, Nov. 2016.

[3] H. Zhang, W. Liu, Z. Chen, G. Luo, J. Liu, and D. Zhao, "Asymmetric space vector modulation for PMSM sensorless drives based on square-wave voltage injection method," *IEEE Trans. Ind. Appl.*, vol. 54, no. 2, pp. 1425–1436, Mar./Apr. 2018.

[4] J. Holtz and N. Oikonomou, "Synchronous optimal pulsewidth modulation and stator flux trajectory control for medium-voltage drives," *IEEE Trans. Ind. Appl.*, vol. 43, no. 2, pp. 600–608, Mar. 2007.

[5] Z. Zhang, X. Ge, Z. Tian, X. Zhang, Q. Tang, and X. Feng, "A PWM for minimum current harmonic distortion in metro traction PMSM with saliency ratio and load angle constrains," *IEEE Trans. Power Electron.*, vol. 33, no. 5, pp. 4498–4511, May 2018.

[6] J. Holtz, G. D. Cunha, N. Petry, and P. J. Torri, "Control of large salient-pole synchronous machines using synchronous optimal pulsewidth modulation," *IEEE Trans. Ind. Electron.*, vol. 62, no. 6, pp. 3372–3379, Jun. 2015.

[7] M. Balasubramonian and V. Rajamani, "Design and real-time implementation of SHEPWM in single-phase inverter using generalized hopfield neural network," *IEEE Trans. Ind. Electron.*, vol. 61, no. 11, pp. 6327–6336, Nov. 2014.

[8] Y. Zhang, Z. Zhao, and J. Zhu, "A hybrid PWM applied to high-power three-level inverter-fed induction-motor drives," *IEEE Trans. Ind. Electron.*, vol. 58, no. 8, pp. 3409–3420, Aug. 2011.

[9] T. Bernardes, V. F. Montagner, H. A. Gründling, and H. Pinheiro, "Discrete-time sliding mode observer for sensorless vector control of permanent magnet synchronous machine," *IEEE Trans. Ind. Electron.*, vol. 61, no. 4, pp. 1679–1691, Apr. 2014.

[10] N. K. Quang, N. T. Hieu, and Q. P. Ha, "FPGA-based sensorless PMSM speed control using reduced-order extended Kalman filters," *IEEE Trans. Ind. Electron.*, vol. 61, no. 12, pp. 6574–6582, Dec. 2014.

[11] Z. Chen, J. Gao, F. Wang, Z. Ma, Z. Zhang, and R. Kennel, "Sensorless control for SPMSM with concentrated windings using multisignal injection method," *IEEE Trans. Ind. Electron.*, vol. 61, no. 12, pp. 6624–6634, Dec. 2014.

[12] H. Zhang, W. Liu, Z. Chen, S. Mao, T. Meng, J. Peng, and N. Jiao, "A time-delay compensation method for IPMSM hybrid sensorless drives in rail transit applications," *IEEE Trans. Ind. Electron.*, vol. 66, no. 9, pp. 6715–6726, Sep. 2019.

[13] P. Dirk, P. Landsmann, S. Kuehland, and R. Kennel, "Arbitrary injection for permanent magnet synchronous machines with multiple saliencies," in *Proc. IEEE ECCE Conf.*, Sep. 2013, pp. 511–517.

[14] Z. Chen, H. Zhang, W. Tu, B. Tan, and G. Luo, "FPGA implementation of an arbitrary injection based sensorless control for PMSM," in *Proc. IEEE Energy Convers. Congr. Expo. (ECCE)*, Sep. 2018, pp. 1741–1747.

[15] Z. Zhao, Y. Zhong, H. Gao, L. Yuan, and T. Lu, "Hybrid selective harmonic elimination PWM for common-mode voltage reduction in three-level neutral-point-clamped inverters for variable speed induction drives," *IEEE Trans. Ind. Electron.*, vol. 27, no. 3, pp. 1152–1158, Mar. 2012.

[16] M. Steczek, P. Chudzik, and A. Szeląg, "Combination of SHE- and SHM-PWM techniques for VSI DC-link current harmonics control in railway applications," *IEEE Trans. Ind. Electron.*, vol. 64, no. 10, pp. 7666–7678, Oct. 2017.

[17] K. Gnanasambandam, A. Edpuganti, A. K. Rathore, D. Srinivasan, C. Cecati, and C. Buccella, "Optimal low switching frequency pulsewidth modulation of current-fed three-level converter for solar power integration," *IEEE Trans. Ind. Electron.*, vol. 63, no. 11, pp. 6877–6886, Nov. 2016.

[18] N. Oikonomou and J. Holtz, "Closed-loop control of medium-voltage drives operated with synchronous optimal pulsewidth modulation," *IEEE Trans. Ind. Appl.*, vol. 44, no. 1, pp. 115–123, Jan./Feb. 2008.

[19] A. K. Rathore, J. Holtz, and T. Boller, "Synchronous optimal pulsewidth modulation for low-switching-frequency control of medium-voltage multilevel inverters," *IEEE Trans. Ind. Electron.*, vol. 57, no. 7, pp. 2374–2381, Jul. 2010.

[20] P. Landsmann, J. Jung, M. Kramkowski, P. Stolze, D. Paulus, and R. Kennel, "Lowering injection amplitude in sensorless control by means of current oversampling," in *Proc. 3rd IEEE Int. Symp. Sensorless Control Elect. Drives (SLED)*, Sep. 2012, pp. 1–6.

ZHE CHEN was born in Huozhou, China, in 1986. He received the B.S. and M.S. degrees from Automation Faculty, Northwestern Polytechnical University (NPU), Xi'an, China, in 2008 and 2011, respectively, both in electrical engineering, and the Dr.-Ing. degree in electrical engineering from the Institute for Electrical Drive Systems and Power Electronics, Technical University of Munich, Munich, Germany, in 2016. Since 2017, he has been an Associate Professor with NPU. His research interests include predictive control and sensorless control for power electronics and electric drives, renewable energy systems, and application of field-programmable gate array-based digital controller.

HANG ZHANG received the B.S. degree in electronic and information engineering from the Hefei University of Technology, Hefei, China, in 2010, and the M.S. degree in detection technique and automatic device from the Xi'an University of Science and Technology, Xi'an, China, in 2013. He is currently pursuing the Ph.D. degree in electrical engineering with Northwestern Polytechnical University, Xi'an. His research interest includes sensorless control and inverter modulation strategy for rail transit permanent magnet synchronous motor drives.

WENCONG TU (S'13) was born in Shaanxi, China, in 1988. He received the B.S. and M.S. degrees both in electrical engineering from Automation Faculty, Northwestern Polytechnical University (NPU), Xi'an, China, in 2011 and 2014, respectively. Since 2013, he has been pursuing the Ph.D. degree in electrical engineering with NPU.

His research interests include predictive control for power electronics and electric drives, real-time simulation technology for electrical drive system, and application of FPGA-based digital controller.

GUANGZHAO LUO received the M.S. and Ph.D. degrees in electrical engineering from Northwestern Polytechnical University (NPU), Xian, China, in 1998 and 2003, respectively. From 2003 to 2004, he was a Postdoctoral Researcher with the University of Federal Defense, Munich, Germany. He is currently a Professor with NPU. In addition, he is the Vice Director of the Rare Earth Permanent Magnet Electric Machine and Control Engineering Center of Shaanxi Province. His research interests include advance control theory of permanent magnet electrical machine, high performance control technology of permanent magnet synchronous motor for electric traction and electric vehicle, real-time simulation technology for electrical drive system, and intelligence control of new energy conversion. He received the China National Defense Science and Technology Progress Award, Second Prize, in 1995 and 2011.

DARSHAN MANOHARAN was born in Fürth, Germany, in 1986. He received the Dipl.-Ing. degree in electrical engineering and information technology from the Technical University of Munich, Munich, Germany, in 2013. Since 2013, he has been a Research Associate with the Institute for Electrical Drive Systems and Power Electronics, Technical University of Munich, Munich, Germany. His research interest includes sensorless control of electrical drives.

RALPH KENNEL (M'89-SM'96) was born in Kaiserslautern, Germany, in 1955. He received the Diploma and Dr.-Ing. degrees in electrical engineering from the University of Kaiserslautern, Kaiserslautern, in 1979 and 1984, respectively. From 1983 to 1999, he worked on several positions with Robert BOSCH GmbH, Stuttgart, Germany. From 1994 to 1999, he was a Visiting Professor with the University of Newcastle upon Tyne, Tyne, U.K. From 1999 to 2008, he was a Professor of Electrical Machines and Drives with Wuppertal University, Wuppertal, Germany. Since 2008, he has been a Professor of Electrical Drive Systems and Power Electronics with Technische Universtät München, München, Germany. His research interests include sensorless control of ac drives, predictive control of power electronics, and hardware-in-the-loop systems. He is a Fellow of the Institution of Electrical Engineers. Within the IEEE, he is the Treasurer of the Germany Section and an Energy Conversion Conference and Exposition (ECCE) Global Partnership Chair of the Power Electronics Society. He is a Chartered Engineer in the U.K.

• • •